symmetry

MDPI

Review

How Transverse Waves Drive Turbulence in the Solar Corona

Thomas Howson

School of Mathematics and Statistics, University of St Andrews, St Andrews KY16 9SS, UK; tah2@st-andrews.ac.uk

Abstract: Oscillatory power is pervasive throughout the solar corona, and magnetohydrodynamic (MHD) waves may carry a significant energy flux throughout the Sun's atmosphere. As a result, over much of the past century, these waves have attracted great interest in the context of the coronal heating problem. They are a potential source of the energy required to maintain the high-temperature plasma and may accelerate the fast solar wind. Despite many observations of coronal waves, large uncertainties inhibit reliable estimates of their exact energy flux, and as such, it remains unclear whether they can contribute significantly to the coronal energy budget. A related issue concerns whether the wave energy can be dissipated over sufficiently short time scales to balance the atmospheric losses. For typical coronal parameters, energy dissipation rates are very low and, thus, any heating model must efficiently generate very small-length scales. As such, MHD turbulence is a promising plasma phenomenon for dissipating large quantities of energy quickly and over a large volume. In recent years, with advances in computational and observational power, much research has highlighted how MHD waves can drive complex turbulent behaviour in the solar corona. In this review, we present recent results that illuminate the energetics of these oscillatory processes and discuss how transverse waves may cause instability and turbulence in the Sun's atmosphere.

Keywords: MHD oscillations; coronal heating; MHD turbulence

Citation: Howson, T. How Transverse Waves Drive Turbulence in the Solar Corona. *Symmetry* **2022**, *14*, 384. https://doi.org/10.3390/sym14020384

Academic Editors: Fabio Reale and Paolo Pagano

Received: 29 November 2021
Accepted: 10 February 2022
Published: 15 February 2022

1. Introduction

1.1. Background

In the decades since Hannes Alfvén published their pioneering analysis on magnetohydrodynamic (MHD) wave modes [1], the Sun's atmosphere has been extensively used as a laboratory for observing, describing and understanding oscillatory behaviour in magnetised fluids. Dissimilar to many other astrophysical plasmas, the Sun is relatively close to Earth and, thus, its atmosphere can be studied in high detail with both ground- and space-based telescopes. Indeed, results provided by contemporary observing facilities consistently highlight the abundance of oscillatory power throughout all regions of the Sun's atmosphere. Continuous monitoring with a high cadence and high resolution, imaging and spectroscopy has identified a plethora of different wave modes permeating the photosphere (e.g., [2,3]), the chromosphere (e.g., [4,5]), the corona (e.g., [6,7]) and solar wind (e.g., [8,9]). The ubiquity of this periodic behaviour provides a range of questions for solar physicists, including:

1. How is wave power transmitted through the atmosphere?
2. To what extent does wave energy contribute to maintaining the atmospheric temperature profile and to accelerating solar wind?
3. Can wave behaviour provide information about the nature of the atmosphere through a seismological analysis?

Each of these questions have been extensively investigated through a range of observational, numerical and theoretical studies. However, due to a range of difficulties, such as observational uncertainties and the inherent complexity of MHD wave behaviour in a dynamic atmosphere, our understanding of these problems remains incomplete. This

review focuses on one key aspect of oscillatory behaviour, which is pertinent to all three of these points; namely, to what extent do transverse MHD waves drive turbulent behaviour in the solar corona?

1.2. Context

The solar corona contains low-density plasma that is maintained at temperatures in excess of 1 million K, despite energy losses due to thermal conduction (to the chromosphere), optically thin radiation and solar wind (which carries energy and mass into Space). The exact processes which maintain these surprisingly high temperatures remain unclear and are the focus of one of the greatest unsolved questions in solar physics; the coronal heating problem (see reviews by [10–17]).

Historically, proposed models for coronal heating have been classified into two broad groups; alternating current (AC) heating and direct current (DC) heating. This dichotomy arises from the characteristic time scales, τ_D, of the photospheric flows that inject energy into the solar atmosphere. For any given coronal structure that has two foot points embedded within the lower atmosphere, the Alfvén travel time, τ_A, is the time taken for a perturbation propagating at the local Alfvén speed to travel along the structure's length, from one foot point to the other. If the characteristic time scales of the photospheric velocities are short in comparison to the travel time ($\tau_A < \tau_D$), we typically find DC heating. However, if $\tau_D > \tau_A$, we typically find AC heating. Classically, DC heating has become synonymous with magnetic reconnection and impulsive heating events, whereas AC heating has been assumed to result in a steadier Ohmic and viscous energy release. However, high-resolution numerical modelling shows that this traditional viewpoint is not so clear cut. This review focuses on this aspect of AC heating, where energy release is intermittent, bursty and driven by turbulent reconnection events (e.g., [18–20]).

Since the launch of the Transition Region and Coronal Explorer (TRACE) instrument [21] in 1998, a range of observational datasets (e.g., [6,7,22–28]) have revealed the proliferation of transverse waves throughout the corona. These were reviewed by [29–32]. Historically, observations of coronal loops have shown rapid damping that is consistent, with energy being transferred from the global mode to local modes in the loop boundary through resonant absorption (see [33] and Section 3). As the wave behaviour and the rate of this damping are well predicted by the linear theory (e.g., [34]), these observations can be used to estimate coronal parameters (such as the magnetic field strength) through seismological techniques [30,35–38]. Whilst the damping process is not necessarily indicative of energy dissipation (as resonant absorption is fundamentally an ideal process [34,39,40]), it does localise energy in small scales, where it is more easily dissipated (e.g., [41–44]). Following this mode conversion, a cross-field gradient in the Alfvén speed also allows phase mixing [45] to occur in the boundary of coronal loops, generating even smaller scales and allowing a more efficient energy dissipation (e.g., [46–50]).

The combined action of resonant absorption and phase mixing in the boundary of coronal density structures results in the formation of large, localised gradients in the velocity fields. This shear can become unstable to the magnetic Kelvin–Helmholtz instability (KHI, e.g., [51]), which disrupts the velocity field through the development of a series of vortices. The oscillatory nature of the system complicates the analysis and reduces the time-averaged shear (compared to a steady flow), but needs not prevent the formation of the instability (e.g., [52–55]). Even in systems which are stable to the KHI, a parametric instability caused by resonance between wave perturbations and the oscillatory forcing (driver) is able to generate small scales, particularly along the magnetic field [56]. For cases where Kelvin–Helmholtz vortices are able to form, a continued instability generates secondary vortices and progressively passes energy to increasingly large wave numbers. This drives an energy cascade towards the dissipation length scale, where mechanical energy is inevitably converted to heat. As such, this process (and any other wave behaviour which forms turbulent-like regimes) is of significant interest to proponents of wave heating in the solar corona.

In addition to observations of rapidly damped oscillations, more recently, there have been many reports of apparently decayless oscillations (e.g., [57–62]), with amplitudes that persist (or sometimes even grow, e.g., [57]) over many wave periods. Typically, these waves are not excited by an external trigger (for example, by a nearby flare), but instead may be driven continuously (e.g., by foot-point velocities). In this case, there is a steady supply of energy to the oscillating structure, which can power continued oscillation and drive wave heating. On the other hand, the analysis of synthetic emission derived from numerical simulations has suggested that these observations could be an apparent effect of the resonant absorption, phase mixing and KHI within the waveguide [63]. The details of these oscillations are discussed in more detail in Section 3.3.

In this review, we consider the latest studies investigating transverse wave-driven turbulence and discuss the implications in terms of plasma heating, the fundamental nature of the solar atmosphere and coronal seismology. In Section 2, we begin with a simple consideration of the energetics of transverse waves, particularly in regard to numerical simulations. Then, in Sections 3 and 4, we discuss models of small-scale generation by standing and propagating waves, respectively. Finally, in Section 5, we present a brief discussion of outstanding questions and problems in this area.

2. Poynting Flux

Due to inherent observational uncertainties, such as the Line of Sight (LoS) integration effects and errors in density measurements, estimates of the wave energy flux in the corona are not well constrained (for example, see different findings in [7,26,64]). Additionally, using non-thermal line widths to appraise the effects of multiple different flows along the LoS can be very unreliable [65,66]. Further, variation between coronal regions (e.g., see Table 1 in [16]) and different energy requirements across the corona [67], makes it difficult to evaluate whether the wave energy flux is sufficient enough to provide significant heating. In practice, whilst the wave energy content may be sufficient to heat the quiet Sun (where energy requirements are relatively low), it seems unlikely that it can balance the losses expected in active region loops or generate the very high temperatures observed here.

Numerical models of coronal heating often assume an imposed velocity driver that moves the foot points of magnetic field lines. This is designed to mimic some aspect of the buffeting motions at the solar surface and can inject energy into the computational domain, which may ultimately be dissipated as heat. We briefly analysed the rate of energy injection. For the following simple arguments, we assumed an initial, uniform magnetic field, $\mathbf{B} = (0, 0, B_0)$, was aligned in the z direction. Each field line had a length of $L/2$ (distance between the upper and lower z boundaries) and the upper z boundary acted as a mirror. Thus, we really considered the field lines of length L that were symmetric about their respective apex. The density, ρ, was uniform. A schematic of this setup is shown in panel (**a**) of Figure 1. We considered a simple sinusoidal wave driver of the form $\mathbf{v}(\mathbf{t}) = (0, v_y(t), 0)$, where:

$$v_y = v_0 \sin \omega t. \tag{1}$$

Here, v_0 is the wave amplitude and ω is the wave frequency. This velocity profile is shown in panel (**b**) of Figure 1 (solid line). The dashed line was obtained from Equation (6) (see below). This imposed velocity excited the Alfvén waves, which propagated along the magnetic field lines with a wavelength of $\lambda = 2\pi v_A/\omega$ (assuming that $\lambda < L/2$), where $v_A = B_0/\sqrt{\mu_0 \rho}$ was the Alfvén speed. If the frequency was too low (and, consequently, the wavelength too large), the wave front reached the upper z boundary before a complete wave cycle was injected. Upon reaching the reflecting boundary, the waves changed direction and began propagating downwards. At the reflected boundary, waves had the form:

$$v_y = v_0 \sin\{\omega t - \phi\}, \tag{2}$$

where $\phi = \omega L/2v_A$ and was associated with a phase shift caused by the travel time along the field lines. The counter-propagating waves then experienced a constructive and destructive interference (according to the local phase shift). At a particular height, $z = z_0$, the upward and downward propagating waves were defined using ϕ_1 and ϕ_2, respectively. These satisfied:

$$\frac{\phi_1}{\omega} = \frac{z_0}{v_A}, \tag{3}$$

$$\frac{\phi_2}{\omega} = \frac{L - 2z_0}{2v_A}. \tag{4}$$

Thus, in the linear, undamped regime, the superimposed wave velocity was given by:

$$v_y = v_0 \sin\left\{\omega\left(t - \frac{z_0}{v_A}\right)\right\} - v_0 \sin\left\{\omega\left(t - \frac{L - 2z_0}{v_A}\right)\right\}. \tag{5}$$

Once the downward-propagating wave reached the driven boundary, it then reflected again, ensuring there was an ever-increasing number of reflections as time progressed. As such, the superposition of an increasing number of waves had to be accounted for to provide:

$$v_y(z,t) = v_0 \sum_{n=0}^{m} (-1)^n H_n(z,t) \sin\{\omega t - \phi_n(z)\}. \tag{6}$$

Here, m is the number of wave reflections that occurred by time, t, $H_n(z,t)$ is 1 if the nth reflection reached a height of z by time, t, and 0 otherwise, and $\phi_n(z)$ is the phase shift associated with the nth wave reflection at a height of z. This can be expressed as:

$$\frac{\phi_n(z)}{\omega} = \frac{Ln}{2v_A} + \frac{z}{v_A} = \frac{Ln + 2z}{2v_A}, \qquad \text{if } n \text{ is even}, \tag{7}$$

$$\frac{\phi_n(z)}{\omega} = \frac{Ln}{2v_A} + \frac{L/2 - z}{v_A} = \frac{L(n+1) - 2z}{2v_A}, \qquad \text{if } n \text{ is odd}. \tag{8}$$

In a similar way, for this Alfvén wave, the magnetic field perturbation was given by:

$$b_y(z,t) = \frac{-B_0 v_0}{v_A} \sum_{n=0}^{m} H_n(z,t) \sin\{\omega t - \phi_n(z)\}. \tag{9}$$

In panel (**c**) of Figure 1, we show some results from this setup with $\omega \approx 6.37\omega_0$, where ω_0 is the fundamental frequency of the system. As this was not an integer multiple of ω_0, this represented non-resonant driving. In panel (**c**), we show the temporal evolution of the perturbed velocity (black) and magnetic fields (red) at $z = L/4$. The solid line shows the results from a numerical simulation and the dashed lines were obtained using Equations (6) and (9). More thorough analyses of similar equations relating to Alfvén waves in a variety of media were presented in (e.g., [68–72]).

At the driven boundary ($z = 0$), once a downward-propagating wave reached this height, a new reflection was created instantaneously. Therefore, for odd n, $H_n(0,t) = H_{n+1}(0,t)$. As such, by isolating the $n = 0$ term (driver) and defining $M = \lfloor m/2 \rfloor$, the upward (n was even) and downward (n was odd)-propagating waves could be separated. Consequently, we could rewrite Equation (6) as:

$$v_y(0,t) = v_0 \sin(\omega t) + v_0 \sum_{n=1}^{M} [\sin\{\omega t - \phi_{2n}(0)\} - \sin\{\omega t - \phi_{2n-1}(0)\}]. \tag{10}$$

As $\phi_{2n} = \phi_{2n-1} = \omega l n / v_A$, all terms in the summation were zero. Reassuringly, this expression reduced to the imposed boundary condition at the lower z boundary. Using

Equation (9), and again considering even and odd n separately, the perturbed component of the magnetic field at $z = 0$ could be expressed as:

$$b_y(0,t) = \frac{-B_0 v_0}{v_A} \sum_{n=0}^{m} \sin\{\omega(t - \phi_n(0))\} \tag{11}$$

$$= \frac{-B_0 v_0}{v_A} \left[\sin\omega t + 2 \sum_{n=1}^{M} \sin\left\{ \omega \left(t - \frac{Ln}{v_A} \right) \right\} \right]. \tag{12}$$

The amplitude of v_y was set by the imposed driving; however, the amplitude of b_y was modified by the reflected waves. It is important to note that, after $t = L/v_A$, when the first of the return waves reached the driven boundary, b_y, and, therefore, the energy injection rate (see below), they were sensitive to both the imposed driver and the nature of the reflected waves. Due to the interference of wave modes, the amplitude of b_y remained bound (for $M \to \infty$), except in the case where the reflected waves were in phase with the wave driving (resonance). This occurred for:

$$\omega = \frac{2\pi k v_A}{L}. \tag{13}$$

for any integer k. For such a frequency, a resonant standing mode would be excited with an amplitude which increased in time, until the linear analysis broke down.

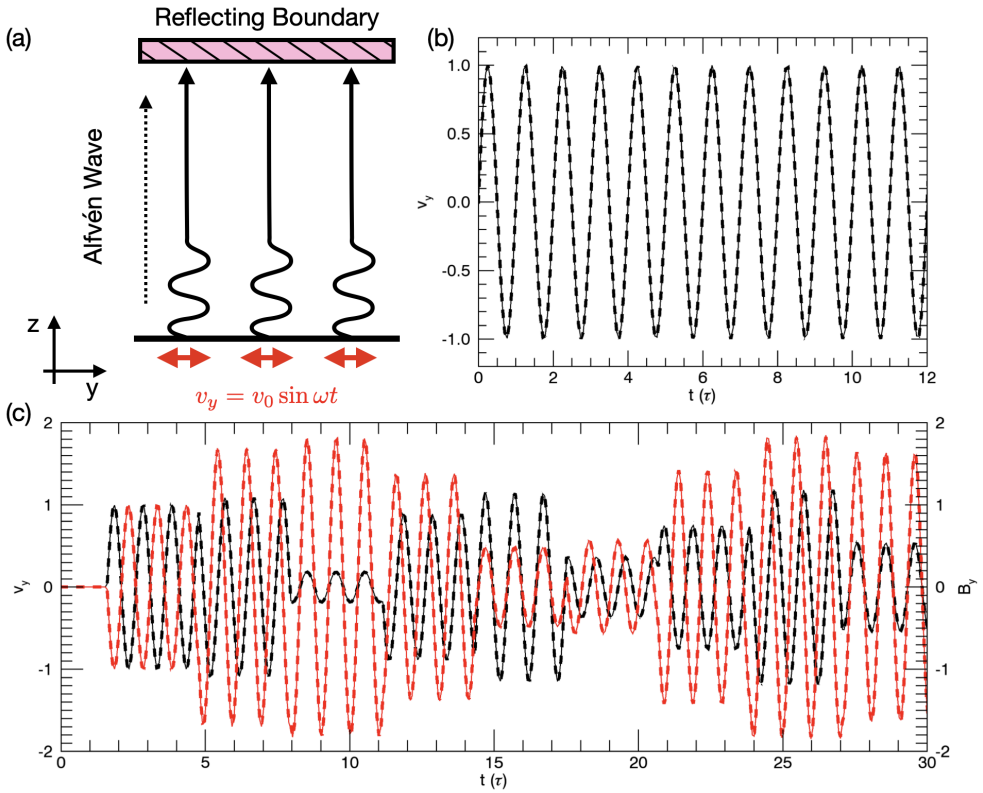

Figure 1. (**a**) Schematic of a simple Alfvén wave excited by an imposed velocity driver and propagating towards a reflecting boundary. (**b**) Imposed wave driver from Equation (2) (solid line) and from Equation (6) (dashed line) (**c**). Perturbed velocity (black) and magnetic fields at $z = L/4$. The solid line shows simulation results and the dashed line was obtained from Equation (9). The case considered here was non-resonant driving with $\omega \approx 6.37\omega_0$.

As a result of the law of energy conservation, the total, volume-integrated energy, E, satisfied:

$$\frac{\mathrm{d}E}{\mathrm{d}t} + \int_S \mathbf{F} \cdot \mathrm{d}\mathbf{S} = 0. \tag{14}$$

Here, the integration was calculated over the boundary, S, of the given volume, and $\mathbf{F}$ was the energy flux. This could be decomposed as:

$$\mathbf{F} = \frac{\rho v^2 \mathbf{v}}{2} + \frac{\gamma P \mathbf{v}}{\gamma - 1} + \rho \Phi \mathbf{v} + \frac{\mathbf{E} \times \mathbf{B}}{\mu_0}. \tag{15}$$

Here, we neglected any thermal conductive flux and the terms on the right-hand side represent the kinetic energy flux, the enthalpy flux, the gravitational potential energy flux and the Poynting flux, respectively. For our given boundary conditions, the perpendicular velocities were zero (or cancelled out across periodic boundaries) and, thus, $\mathbf{v} \cdot \mathrm{d}\mathbf{S} = 0$. As such, the change in total energy reduced to:

$$\frac{\mathrm{d}E}{\mathrm{d}t} = -\frac{1}{\mu_0} \int_S \mathbf{E} \times \mathbf{B} \cdot \mathrm{d}\mathbf{S} \tag{16}$$

$$= -\frac{1}{\mu_0} \int_S \{\eta(\nabla \times \mathbf{B}) \times \mathbf{B} - (\mathbf{v} \times \mathbf{B}) \times \mathbf{B}\} \cdot \mathrm{d}\mathbf{S}. \tag{17}$$

In the ideal limit ($\eta \to 0$), this would reduce further to leave:

$$\frac{\mathrm{d}E}{\mathrm{d}t} = \frac{1}{\mu_0} \int_S (\mathbf{v} \times \mathbf{B}) \times \mathbf{B} \cdot \mathrm{d}\mathbf{S} \tag{18}$$

$$= \frac{1}{\mu_0} \int_S \{(\mathbf{B} \cdot \mathbf{v})\mathbf{B} - (\mathbf{B} \cdot \mathbf{B})\mathbf{v}) \cdot \mathrm{d}\mathbf{S}. \tag{19}$$

Here, the first term represents the driving of the existing flux by the imposed velocity and the second term represents the emergence/submergence of the new flux. Again, since $\mathbf{v} \cdot \mathrm{d}\mathbf{S} = 0$, the second term vanished, and for the current geometry and wave driver, we were left with:

$$\frac{\mathrm{d}E}{\mathrm{d}t} = \frac{-1}{\mu_0} \int_S B_y v_y B_z \, \mathrm{d}x\mathrm{d}y, \tag{20}$$

where the integral was calculated over the surface of the driven boundary [12]. The implications of this equation are shown in Figure 2. When the velocity driver increased the angle between the magnetic field and the surface's normal vector, the energy would be injected. Otherwise, energy would be removed from the system.

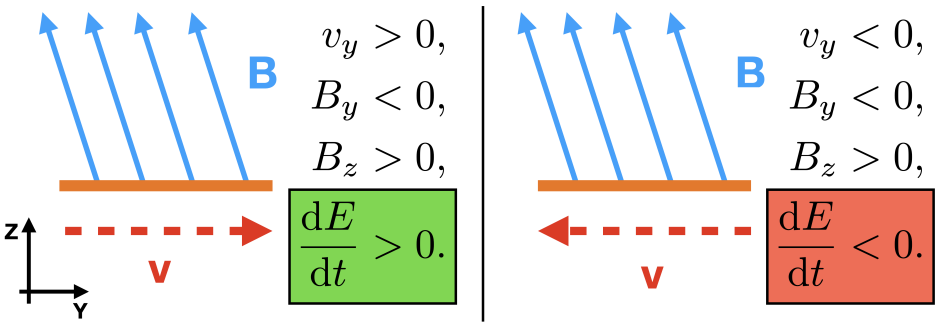

Figure 2. Schematic of the Poynting flux associated with velocity driving on magnetic foot points. Details in Equation (20). Adapted from Figure 5 in [73].

For the wave described above, we could evaluate the Poynting flux using Equations (10) and (12), and taking $B_z = B_0$, the initial field strength. We found:

$$\frac{\mathrm{d}E}{\mathrm{d}t} = \frac{AB_0 v_0^2 \sqrt{\rho_0}}{2\sqrt{\mu_0}} \left[\sin^2 \omega t + 2 \sum_{n=1}^{M} \sin \omega t \sin \left\{ \omega \left(t - \frac{Ln}{v_A} \right) \right\} \right], \tag{21}$$

where A is the area of the driven boundary and we used $v_A = B_0/\sqrt{\mu_0 \rho_0}$. The first term in the square brackets was always positive and represented the energy injected before any reflections reached the lower boundary. The second term was associated with the complex interaction between the driver and the reflected waves. It was always positive for resonant driving (see Equation (13)), but otherwise, the time averaged contribution (over long times) was 0. The implications of Equation (21) are outlined in Figure 3. We showed the instantaneous (left-hand column) and cumulative Poynting flux (right-hand column) for non-resonant (upper row) and resonant (lower row) driving. In the right-hand panels, we compared the results of simulations (solid lines) with the predictions from the time integral of Equation (21) (dashed lines). In panel (**a**), we saw that the Poynting flux could be both positive and negative (above or below the dashed horizontal line) for non-resonant driving, resulting in a much lower average rate of energy injection than for the resonant case. In panel (**c**), we saw that the resonant driving led to an approximately linear increase in the instantaneous Poynting flux as time progressed. This resulted in the quasi-quadratic evolution in panel (**d**).

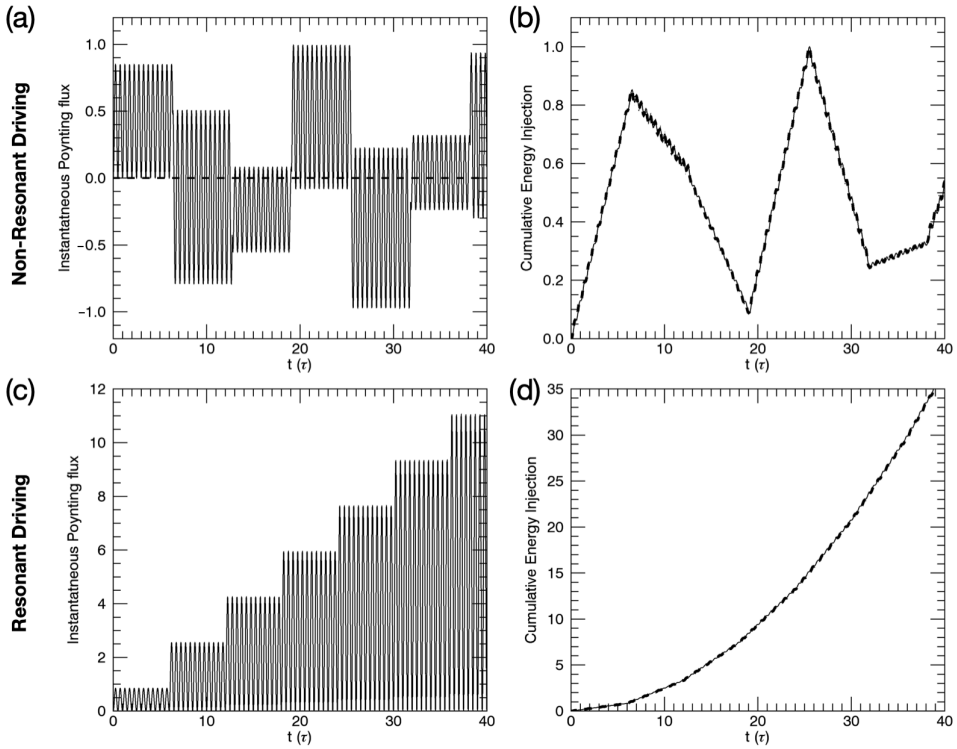

Figure 3. (**a**,**c**) Evolution of the instantaneous Poynting flux for $\omega \approx 6.37\omega_0$ (non-resonant driving) and $\omega = 6\omega_0$ (resonant driving), respectively. The solid dashed line in (**a**) shows an energy injection rate of 0. (**b**,**d**) The cumulative energy injection for non-resonant and resonant driving, respectively. Solid lines show simulation results and dashed lines were obtained using the time integral of Equation (21).

It is important to note that Equation (21) only applies for undamped, sinusoidal waves with a perfect reflection at the upper z boundary. If any of these conditions were broken, then the wave driver was able to inject more energy into the system. For example, AC driving, which forces the evolution of the background field, was able to sustain a larger

Poynting flux (e.g., [74]). Additionally, if the downward propagating wave had a lower amplitude than the driver, a long-term positive influx of energy was permitted. This may be associated with wave energy dissipation or would be the case in open-field regions, where only a partial reflection due to longitudinal stratification is possible. As such, it is clearly important to understand the wave dynamics away from a driven boundary. It is not sufficient to merely observe wave amplitudes at the base of the corona in order to determine the efficacy of wave heating. Indeed, the interaction with wave energy already in the corona could have significant effects on the energy flux (e.g., [10]).

3. Standing Modes

The magnetically closed corona consisted of field lines which were connected to the lower layers of the solar atmosphere at two distinct foot points. This meant that each foot point could be driven independently, which could have important consequences for the wave behaviour on these field lines. The density structures observed in the corona were typically assumed to outline the structure of the magnetic field, and in the closed corona, would often form coronal loops. These approximately semi-circular structures are important in the context of MHD wave dynamics, as they act as wave guides for oscillatory phenomena. These waves can be trapped within the coronal volume of a loop due to the large density gradients that exist close to the magnetic foot points in the transition region. As a result, standing wave modes are often observed in the Sun's corona and these can be particularly adept at driving MHD turbulence.

Some of the first coronal waves observed in the corona were large scale, transverse motions that displaced the central axis of a coronal loop [6,22]. As the displacement at the loop apex was much larger than at the loop foot points, these were interpreted as standing waves, and, in particular, standing kink waves. These waves are often described by assuming a long, thin, azimuthally invariant cylindrical tube with a relatively high density, embedded in a lower-density plasma (e.g., [30]).

The kink speed, c_k, of a wave in this tube could be expressed as a density-weighted geometric average of the interior and exterior Alfvén speeds. It was given by:

$$c_k = \sqrt{\frac{\rho_i c_{A_i}^2 + \rho_e c_{A_e}^2}{\rho_i + \rho_e}}, \tag{22}$$

where $c_{A_{i,e}}$ is the local Alfvén speed, $\rho_{i,e}$ is the density and the subscripts i and e refer to interior and exterior quantities, respectively, (e.g., [32,75]). We noted that for $\rho_e < \rho_i$ then $c_{A_e} > c_k > c_{A_i}$. Therefore, if we assumed the density varied smoothly across the boundary of the magnetic cylinder, then on some radial shell, the local Alfvén speed would equal the kink speed of the flux tube. As such, a natural resonance would exist, which would allow the transfer of energy from the global, large-scale kink mode, to smaller-scale azimuthal Alfvén waves, which were oscillate on this radial shell. This process is known as mode coupling (for propagating modes) or resonant absorption (for standing modes), and has been well studied with both analytical and numerical treatments (e.g., [33,34,39,40,76–78]). Additionally, this process is very robust and occurs in both curved and straight loops, structures with elliptical cross-sections, various magnetic topologies and with or without the presence of gravity (e.g., [79–84]).

As the azimuthal waves form preferentially on a narrow shell in the cylindrical structure, they are typically associated with relatively large gradients (in cylindrical geometry: $\partial v_\phi / \partial r$). Additionally, as there is a cross-field gradient in the natural Alfvén frequency, phase mixing would further enhance these radial gradients. For standing modes in cylinders with a uniform magnetic field, these gradients could become unstable to the magnetic Kelvin–Helmholtz instability [51]. This velocity shear instability led to the formation of vortices in the velocity field and, ultimately, the large-scale deformation of the density structure. A schematic of this process is shown in Figure 4.

This process was considered analytically in the context of wave heating and phase mixing by [53]. More recently, further analytic work presented in [56] described the instability criteria for a discontinuous oscillatory shear in Cartesian geometry (similar to panel **d** in Figure 4). The analysis assumed a density of ρ_+ on one side of the shear layer and ρ_- on the other. For equal wave frequencies on either side of the velocity shear, the system was unstable would be (reworked from [56]):

$$(\Delta v)^2 > \frac{4k_z^2(\rho_+ + \rho_-)v_{A,+}^2}{\rho_- k_y^2}, \tag{23}$$

where Δv is the difference in the amplitude of the Alfvén waves and $v_{A,+}^2$ is the background Alfvén speed in the $\rho = \rho_+$ region. The wave numbers k_y and k_z were in the direction of the Alfvén wave polarisation and parallel to the background field, respectively. Ultimately, the system was unstable if the velocity shear was large enough to overcome the suppressive effects of magnetic tension. In the case $k_z \to 0$ (increasingly long wave lengths along the field), the tension force changed to zero and the system was always unstable (e.g., [55]). The results of a numerical simulation showing the KHI developing across an oscillatory shear layer are shown in Figure 5. The panels show the disruption of the density profile as the instability developed.

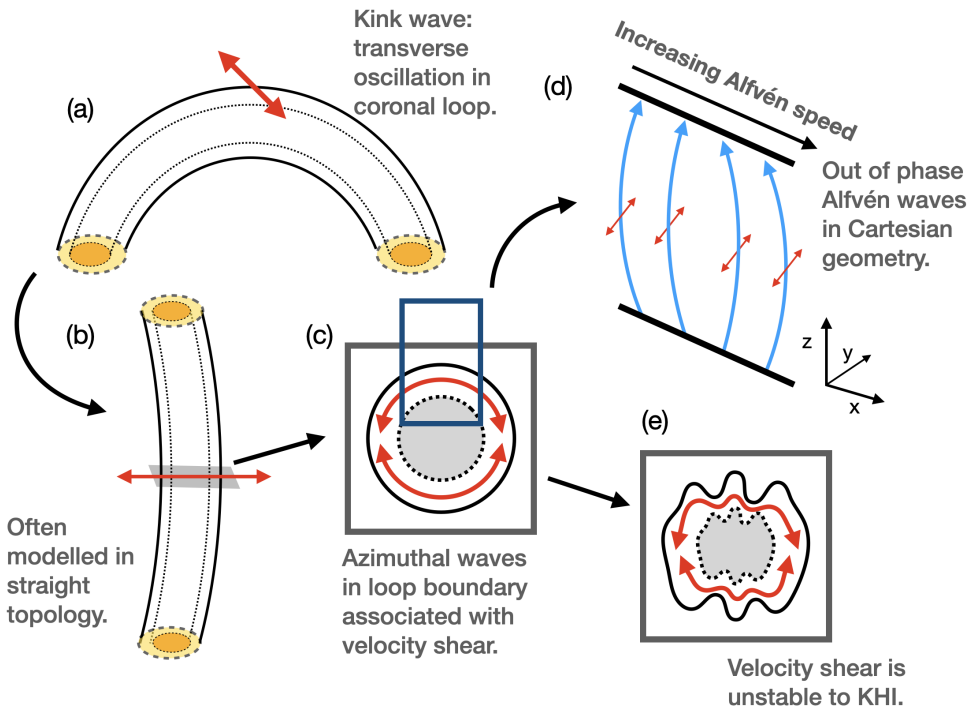

Figure 4. Schematic of KHI formation in transverse standing mode oscillations. (**a**,**b**) Transverse motions observed in coronal loops were interpreted as standing kink modes. (**c**) Resonant absorption led to the localisation of wave energy in the boundary of the coronal loop. (**d**) Phase mixing led to out-of-phase azimuthal Alfvén waves in the loop boundary. (**e**) The velocity shear could become unstable to the KHI. Adapted from Figure 1 in [85].

Many authors have described the development of the instability using numerical simulations with three-dimensional MHD codes. For the case of coronal kink waves, the first numerical simulations were presented by [54]. The authors found that the development of the instability was sensitive to the thickness of the tube boundary between the interior and exterior plasma and to the amplitude of the transverse wave motions. In many subsequent studies, this process has been shown to be robust across a wide parameter space. In particular, it can occur in a variety of atmospheric features such as coronal loops

(e.g., [86]), prominences [87] and spicules [88], in multi-stranded loops [89], in radiatively cooling loops (e.g., [90]) and in gravitationally stratified structures (e.g., [91]).

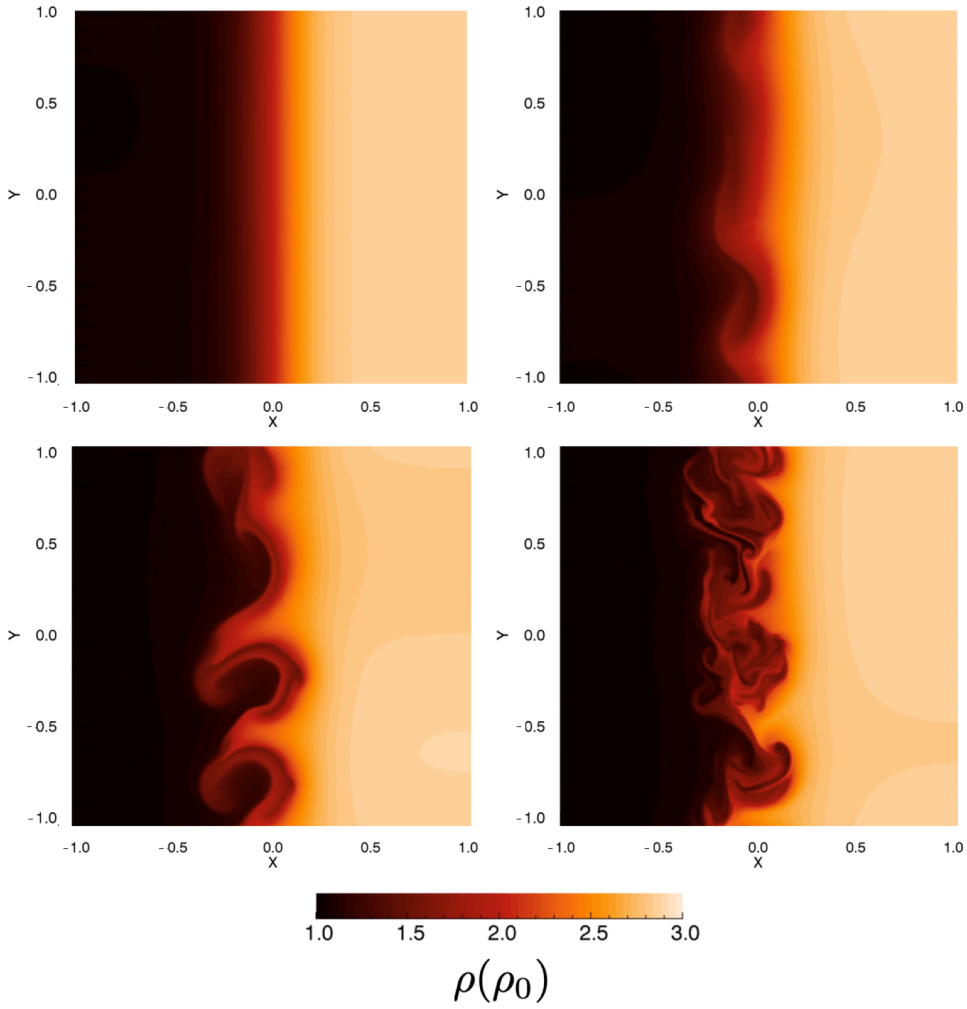

Figure 5. Disruption of the density profile during the formation of the magnetic Kelvin–Helmholtz instability.

For a fundamental standing kink mode (with wave nodes at the two foot points and an antinode at the loop apex), the velocity shear which drives the instability is largest at the loop apex. As such, the deformation in the density cross-section is greatest in the apex plane, and is typically very small close to the foot points. However, the Kelvin–Helmholtz vortices stretch longitudinally along much of the length of the oscillating flux tubes and, thus, a large fraction of the loop volume can be disrupted by the instability. The characteristic vortices that form as the instability develops have been named in the literature as TWIKH (transverse wave-induced Kelvin–Helmholtz) rolls, and are associated with small scales in both the velocity and magnetic fields (as the field is approximately frozen into the plasma). The generation of these small scales can be tracked using the vorticity (for the velocity field) and the current density (for the magnetic field) and, in non-ideal regimes, they lead to viscous and Ohmic heating. Since the perturbed velocity field is largest at the wave antinodes, viscous wave heating occurs, preferentially, at the loop apex (for a fundamental standing mode). Equally, the perturbed magnetic field is largest at the loop foot points (wave nodes) and, thus, Ohmic heating rates tend to be largest here (e.g., [83,92,93]). For the case of the KHI in standing kink modes, ref. [94] presented detailed results showing that the instability generated more Ohmic than viscous heating, but any irreversible temperature increase could be masked by the mixing of non-isothermal

plasma within the Kelvin–Helmholtz vortices. More recently, ref. [85] quantified the rates of magnetic reconnection that is able to occur across an oscillatory shear layer as a result of the onset of the KHI. This was found to be largest when the instability growth rate was greatest, e.g., for long field lines with no shear in the magnetic field (twist in the case of cylindrical geometry).

3.1. Wave Excitation

During the development of the instability, energy cascades to increasingly small scales, until it, inevitably, dissipates (in non-ideal plasmas). As such, the KHI is interesting in the context of coronal wave heating as it enhances the energy dissipation rate. However, the energy content in standing kink modes can be quite small and may, therefore, be insufficient to significantly contribute to the coronal energy budget. This is especially true for impulsively driven waves such as standing kink modes that are excited by a nearby impulsive event (e.g., solar flare). Numerical models of such a case typically provide an initial perturbation which contains all of the wave energy. Not only is this initial energy unable to provide substantial heating, ref. [95] showed that if the instability forms at the boundary of a prominence, the mixing of cold, dense plasma with much hotter and more tenuous coronal plasma can cause an increase in the radiative losses and, thus, lead to enhanced cooling. This increase in the energy loss rate is much larger than the energy dissipation that could be obtained due to the relatively low wave energy content.

On the other hand, kink waves can be driven by continuous foot-point driving, which provides a persistent source of energy to the system (e.g., [93,94]). For such models, transverse modes are often excited by an oscillatory driver with a frequency that matches the natural fundamental kink frequency of the system (e.g., [96]). This resonant driving efficiently injects energy into the coronal volume and, thus, provides a greater chance of substantial plasma heating (see Section 2). In this way, for the first time, ref. [97] presented a wave heating model which was able to balance the radiative losses from the loop once the instability developed. Despite this positive numerical result, ref. [98] presented analytic arguments to show that, for the amplitude of kink modes observed in the corona, there is insufficient energy to balance the expected energy losses.

A simple, continuous sinusoidal driver of the form described in Equation (1), or those used for resonantly exciting standing kink modes, is unlikely to be particularly representative of the complex motions that are observed at the solar surface. Consequently, it remains unclear whether systems driven continuously with a sinusoidal velocity profile are really applicable to the corona. In response to this criticism, recent work has focussed on determining how standing kink modes can be excited by other means. For example, ref. [99] showed how an imposed driving consisting of a range of different frequencies could excite a standing kink mode due to preferential energy injection at resonant frequencies. More recently, this work was extended in [99] to show how random driving could produce a similar effect. Further possibilities have since been described by [100,101], which show how steady flows in the photosphere and corona, respectively, can excite kink oscillations. Regardless of the excitation mechanism, in all of these cases, the Kelvin–Helmholtz instability and the associated cascade of energy to small scales were able to develop. The damping time of a fundamental standing kink mode is strongly affected by the rate at which energy is transferred to azimuthal Alfvén waves in the boundary of the oscillating flux tube (resonant absorption [33]). This is an ideal process which progresses with or without the development of the Kelvin–Helmholtz instability. The linear theory provides expressions for the damping time of the global kink mode, which can be used to derive seismological estimates from coronal observations. However, ref. [102] showed that the onset of the KHI changes the kink mode damping time by modifying the resonant shell in the loop boundary. As such, this raises questions about the validity of seismological estimates if the instability develops in the corona.

In the absence of a smooth density transition across the boundary of an oscillating flux tube, resonant absorption is unable to progress (at least initially, there is no resonant layer of

field lines). The authors of ref. [103] exploited this to determine how the KHI develops both with and without the simultaneous progression of resonant absorption. The authors found that the instability could develop in either case; however, the nature of the vortices was modified when resonant absorption was not permitted. In the classical case (with resonant absorption), small azimuthal wave numbers (large vortices) had the fastest growth rates and, thus, formed before higher wave number modes (smaller vortices). However, when no smooth boundary layer was included, an apparent inverse energy cascade developed with smaller vortices forming first before larger vortices, caused widespread disruption to the loop cross-section. In this case, the formation of the K–H vortices allows resonant absorption to commence, with energy being localised within the mixing layer. As such, even in the case where no resonant absorption is initially possible, the instability generates an evolving resonant layer which allows the energy transfer to occur. The authors showed that resonant absorption is an important process that promotes the spread of wave-driven turbulence throughout an oscillating structure.

3.2. Instability Growth Rate

The growth rate of the KHI in MHD simulations is sensitive to a variety of physical (as shown in Equation (23)) and numerical factors. Firstly, the magnitude of the wave perturbation is significant, with larger amplitude waves generating TWIKH rolls sooner and leading to an increased loop disruption (e.g., [54,90]). Indeed, for continuous resonant driving, the entire loop cross-section is readily deformed by the instability (e.g., [93]). Secondly, the loop-aligned wave number is an important property that can modify the growth rate of the instability through the action of the magnetic tension force (e.g., [56,85]). Given the large length of coronal loops, this is typically a low number, and the magnetic tension is small. Indeed, the assumption $k_{\parallel} \to 0$ is often determined for simplicity (e.g., in the analysis presented by [52]). However, the magnetic tension force is able to delay the onset of the KHI (in terms of wave periods) and reduce the density disruption for shorter loops (e.g., [85]). We note that, as the period of fundamental mode is reduced for shorter field lines, the instability can actually happen sooner for shorter field lines, and it is only delayed in terms of the number of wave periods.

Additionally, as energy dissipation extracts energy from the wave and reduces the velocity shear which drives the instability, increasing the resistivity and/or viscosity reduces the growth rate of the instability. Indeed, for particularly large values, the instability can be suppressed entirely [104]. Due to computational constraints, the magnetic and viscous Reynolds numbers that can be obtained in 3D MHD numerical simulations are typically many orders of magnitude larger than expected for coronal plasmas. As such, the instability growth rate in the corona may be much higher than is obtained in simulations. To this end, as accurate modelling of the non-linear development of the KHI demands extremely high spatial resolution, it is important to note that the instability is likely to be artificially suppressed in a range of numerical simulations.

One further effect that can significantly reduce the growth rate of the instability is twist in the magnetic field [85,105–107]. This effect is particularly profound for loops with thick boundary layers [106]. Classical TWIKH rolls form longitudinal structures that run parallel to the loop axis. For a twisted field, such a formation is restricted as twisted magnetic field lines pass through multiple K–H vortices. This would generate large magnetic tension forces, preventing the independent evolution of each vortex. The TWIKH rolls that manage to form are aligned with the twisted field; however, even for a relatively low twist, they can be much smaller than the vortices that form in corresponding, untwisted cases (e.g., [105]). As such, the density deformation is significantly reduced in twisted loops, which reduces the likelihood of being able to observationally identify the instability in the solar corona (see below).

Whilst a simple azimuthal component in the magnetic field can reduce the growth rate of the instability, it remains unclear whether more complex magnetic fields have a similar (or even more restrictive) effect. The coronal field is very difficult to measure directly and,

as such, its exact nature remains poorly constrained. Despite this, the constant motions observed at the solar surface, coupled with the very low dissipation, suggest that the coronal field should exist in a highly stressed state (e.g., [108]). If this is the case, and if this complex field acts in a similar way to the simply twisted magnetic field, then it is possible that KHI-driven turbulence is not as widespread in the corona as many numerical models might suggest. As an example, in [109], the authors simulated transverse waves injected into a complex and highly inhomogeneous magnetic field. Despite high-amplitude waves forming as a result of localised resonances, no evidence of TWIKH rolls was detected.

3.3. Observational Considerations

Despite the large number of numerical studies predicting the development of KHI-driven turbulence in transversely oscillating coronal loops, direct observational evidence of this mechanism remains lacking. Indeed, a recent study of large amplitude oscillations found no clear evidence of KHI development [110]. Whilst there are undoubtedly several reasons for this, the most pressing probably concerns the spatial resolution afforded by contemporary telescopes. In MHD simulations of the KHI, the smallest scales are determined by the numerical grid size and/or the magnitude of dissipation terms. For the Sun, the smallest scales are bound by the dissipation length scale, which is likely much smaller than the smallest lengths seen in simulations. More pertinently, it remains much smaller than the resolution attained by even the most state-of-the-art telescopes.

In [63,111], the authors generated a synthetic emission from the results of high-resolution numerical simulations of the KHI forming in transversely oscillating structures. By degrading the spatial resolution of the emission to the levels obtained by high-resolution missions (e.g., Hi-C; Figure 11 in [111]), the authors showed that it can be difficult to definitively identify the TWIKH rolls in the imaging data. Given this result was derived from simulations with relatively low Reynolds numbers (in comparison to coronal values), which artificially restrict the cascade to small scales, for real coronal observations, this issue is likely to be exacerbated. Not only is the spatial resolution a significant issue, but LoS effects (due to the optically thin plasma) can mean the emission is integrated across several K–H vortices. This further obfuscates observations and can lead to different results from different LoS, according to the angle between the oscillation polarisation and the viewing direction.

Despite these difficulties, the authors point out there are some characteristic signatures of the wave dynamics which could be detected with the highest resolution instruments (e.g., Hi-C). These include out-of-phase behaviour between the intensity and Doppler velocity oscillations, periodic loop broadening (at twice the oscillation frequency) and an increase in line-broadening as the KHI develops, particularly in the loop boundary where the effects are greatest. For coronal loops that have a cross-field temperature structure, the different dynamics between the loop core and the loop boundary may be detected by considering different spectral lines. In [63], the authors demonstrate that the evolution of resonant absorption, phase mixing and KHI can match the appearance of decayless oscillations in the corona. Additionally, the authors show that the localisation of energy at small scales along with LoS integration effects, can lead to a significant underestimation of the total wave energy from an observational analysis. As such, there may be as much as an order of magnitude more energy than can be measured directly.

More recently [112] presented results which confirmed the difficulty in accurately estimating the wave energy flux from synthetic observations derived from simulations of the KHI induced by transverse oscillations. Once again, the authors demonstrated that the complex wave dynamics produce signatures of decayless oscillations. However, the observed amplitude of these oscillations only showed a weak correlation with the strength of the wave driving. An extra complication for interpreting observations (either synthetic or real) arises from the effects of background emission, as investigated in [113]. In order to compare with real observations, the authors transformed simulations of transverse oscillations in a straight loop into semi-circular structures. In this geometry, they

found that the contribution from the background emission could drastically decrease the measured Doppler velocities and, thus, lead to significant errors in estimates of the wave energy content.

In [114], the authors considered an additional effect of TWIKH rolls on observational data. In particular, they showed that the differential emission measure (DEM) is broadened when a coronal loop is driven continuously and significantly deformed by wave-driven turbulence. Broad DEMs have been identified in observational data and had previously been assumed to be associated with multi-stranded loops (e.g., [115,116]). This result is particularly important in the context of recent studies, which show that multi-stranded loops can be unstable to any transverse oscillation and, thus, may not be able to persist in the corona (see [117] and Section 4).

In a pair of articles, [87,118] presented observational results of transverse oscillations in a prominence together with the numerical modelling of this scenario. With a sophisticated combination of observational and numerical works, the authors interpreted phase differences between plane-of-sky motions and LoS Doppler velocities as evidence of the wave behaviour described in this review (e.g., resonant absorption, phase mixing and KHI evolution). The authors also observed a general shift from emission in cooler chromospheric spectral lines to hotter coronal lines. At the time, this was posited as evidence for wave heating in action. However, a later study by [95] argued this was not a result of energy dissipation, but was instead caused by the mixing of hot coronal plasma with a cooler prominence material. This leads to an average temperature increase in the prominence boundary, causing the transfer of emission from cooler to hotter lines. Despite this, the observations remain of significant interest, as they potentially provide evidence of the instability developing in the solar corona.

4. Propagating Waves

Hitherto, we restricted our attention to the case of standing transverse oscillations. However, propagating modes are also very important in the solar atmosphere (e.g., [27,28,119,120]). Clearly, this is particularly true for open-field regions, where there is no second foot point to aid wave reflection or generate counter-propagating modes from oscillatory driving. However, propagating transverse waves have also been observed in closed structures. Indeed, an analysis of the wave power observed in closed-field regions, showed a disparity between the power associated with the inward (Sun-ward) and outward-propagating waves (e.g., [121,122]). In particular, results showed a greater power for the outwardly propagating oscillations. This is indicative of energy being lost by the wave mode as it travels along field lines. Whilst this could be evidence of energy dissipation, it could also represent a transfer of energy to difficult-to-observe modes (e.g., through resonant absorption [121]) and, thus, not directly showing wave heating.

As coronal loops have two magnetic foot points, different wave modes can be excited at both ends. If these different wave modes each propagate along the loop, at some point they encounter one another. In the linear wave regime, these waves can experience constructive and destructive interference, depending on the relative phase shifts (see Section 2), but the full wave behaviour simply remains the sum of the two individual wave modes. However, in the non-linear regime, the wave modes are able to interact in a complex manner, leading to a cascade of energy to increasingly small scales. It has long been established that this non-linear interaction can induce the development of MHD turbulence (e.g., [123–126]) and, thus, generate the transfer of energy to small scales. For closed coronal field lines, it is clear how the required propagating modes can be generated. Simply exciting different non-linear wave modes from each of the two magnetic foot points is sufficient to set this process in motion (e.g., [127–129]). Although counter-propagating modes may be trivial to generate within closed structures, they are perhaps more frequently studied in open-field topologies. In these cases, given the absence of a second foot point, counter-propagating wave modes must be generated within the structure. Many studies (e.g., [130–132]) have shown that this is possible due to the reflections caused by longitudinal density structuring

(e.g., associated with gravitational stratification). As a result, the decay of propagating Alfvén waves into turbulent-like regimes has been shown to be a promising mechanism for accelerating and heating solar wind (e.g., [128,133–139]). In particular, ref. [140] showed that longitudinal variations in the density can generate an energy cascade that may sustain the temperature of open-field regions if the fluctuations are sufficiently large. The authors found that variations in the density of the order, 24% were sufficient. The role of MHD waves in open-field regions are explored more thoroughly in reviews by [141–143].

Solar wind is a particularly useful laboratory for testing and confirming theories in MHD wave behaviour (e.g., see review by [144]). This is because, unlike closed-field regions, it is accessible for in situ monitoring by near-Earth satellites at 1AU and, more recently, in the inner heliosphere by the Parker Solar Probe and Solar Orbiter, for example. This has allowed models of solar wind to be constrained by measurements at different radial distances to the Sun. In particular, the characteristics of MHD turbulence in solar wind are continuously being investigated (e.g., [145–149]), and very recent results show signatures of wave-driven turbulence extending much closer to the Sun [9,150–152].

In the context of this review, it is important to note that propagating modes are typically stable to the KHI (e.g., [53]). As such, this avenue to wave-driven turbulence is not available to propagating waves. Therefore, propagating Alfvén waves in a homogeneous medium do not drive an energy cascade to small scales. However, in an inhomogeneous medium, the wave dynamics are not so straightforward. The Alfvén fast and slow modes are no longer decoupled and waves can have mixed properties (for example, the kink mode has mixed wave properties, e.g., [153]). One consequence of this increased complexity is that unidirectional waves are able to drive turbulence in non-uniform media.

This was demonstrated using numerical simulations by [117,154]. The authors modelled an inhomogeneous corona that was perturbed by transverse, unidirectional and propagating waves. Within a few hundred seconds, the initial prescribed density profiles were completely deformed by the wave behaviour. As with the standing modes (discussed in Section 3), this led to a proliferation of current sheets throughout the waveguide. This process, which has since been referred to as uniturbulence, may be important for wave heating in the corona, as it significantly expands the set of conditions which permit turbulent development. As transverse waves permeate the solar atmosphere, this suggests that multi-stranded loops may not exist in the corona as they would quickly be disrupted by wave-induced turbulence [117]. An example of this principle is shown in Figure 6. However, it remains possible that sub-strands within a coronal loop are stabilised by a structure within the magnetic field (e.g., [109]).

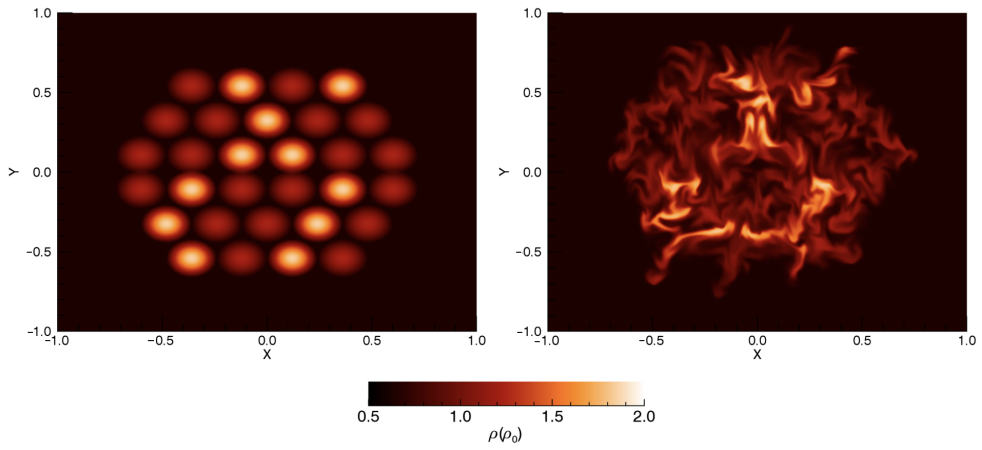

Figure 6. Disruption of the coronal loop strands as a result of uniturbulence (e.g., [117]).

Uniturbulence has since been studied in more depth with analytic treatments [155,156] involving a description of the perturbations with Elsässer variables [157]. These studies have emphasised the importance of the perpendicular structuring on the energy cascade

and, thus, the wave heating rate. This analytic approach has also been extended to compute the damping rates for standing modes accounting for the non-linear evolution of the KHI [158]. In this study, the authors showed that the wave damping time is inversely proportional to the amplitude of the kink mode. This is in agreement with observational results showing that high-amplitude coronal kink waves dampen at a faster rate than low-amplitude oscillations [159–161].

Further numerical simulations of propagating transverse waves excited by continuous boundary motions also show that wave driving can significantly disrupt a pre-existing density structure [162]. In this case, the evolution of the density profile permits wave energy dissipation over a large cross-sectional area, and not just the initial boundary of the loop. This is a positive result in view of the criticism outlined in [163], that wave heating is not able to dissipate energy throughout the loop nor sustain the assumed density profile. However, whilst the heating in such simulations can be significant for some configurations, it has not been able to balance radiative losses in a dense flux tube [50,162], even for highly enhanced dissipation coefficients. Further, it remains unclear whether similar wave driving can support any form of density structure in a fully stratified atmosphere (e.g., [163,164]).

5. Discussion

In a range of physical fluids, high Reynolds number regimes often encourage the formation of turbulence. As such, it may be of little surprise that recent modelling, alongside previous analytical results, has suggested that coronal loops need little encouragement to become turbulent. This review presented a series of studies in which transverse waves drove an energy cascade to small scales in various atmospheric structures, such as loops, prominences and spicules. These results consistently show that, even for the relatively low Reynolds numbers that can be attained in large-scale numerical simulations, it is remarkably easy to encourage the formation of MHD turbulence, e.g., due to the onset of the Kelvin–Helmholtz instability. In the low dissipation corona, we can only expect these non-linear effects to be even more significant, further promoting the development of turbulence in the plasma. If this is indeed the case, there are implications across a wide range of solar physics, not least for wave heating and coronal seismology.

Three substantial and outstanding problems for wave heating models are:

1. Are coronal waves associated with sufficient energy to heat the atmospheric plasma and power solar wind?
2. Can wave heating self-consistently create and sustain the density profile assumed in wave heating models?
3. Are heating rates too low in very high Reynolds number regimes?

As we have seen, wave-driven turbulence has significance for each of these questions. Firstly, LoS integration effects through a turbulent region can lead to large uncertainties in observational measurements. This ensures that estimating the wave energy flux is particularly difficult if the coronal plasma is in a turbulent state. The second question is a major problem with wave heating models highlighted in [163]. However, the disruption of any pre-defined density profile by turbulent flows ensures that wave heating can occur throughout the cross-section of a coronal structure and is not confined to the boundary where Alfvén speed gradients are largest (e.g., for more efficient phase mixing). This is positive in terms of the second question, although it remains to be seen if wave heating is ever able to sustain coronal density structures in a stratified atmosphere. Thirdly, due to computational constraints, investigating high Reynolds numbers coronal plasmas remains very challenging. However, the onset of turbulence enhances energy dissipation rates and, thus, is certainly promising for wave heating. The energy cascade to small scales that develops as a result of these processes is an essential component of many wave heating models. In closed coronal loops, unless waves are driven resonantly, or strongly dissipated, simple sinusoidal drivers do not inject sufficient Poynting flux to balance the expected energy losses (e.g., [71]). As resonant driving quickly excites large-amplitude flows, even in this case, significant damping (and ultimately dissipation) must occur, as

very large-amplitude waves have not been observed. For non-resonant sinusoidal driving, it is important to note that the imposed velocity removes, on average, reflected wave energy at the same rate as new energy is injected, unless the reflected waves have lower amplitudes (e.g., due to dissipation) than the imposed velocity. As such, the rate of energy injection (Poynting flux) is very sensitive to the rate of energy dissipation [10]. Whilst resonant absorption [33] and phase mixing [45] can enhance dissipation rates by localising wave energy, in the classical regimes, they do not typically provide sufficient energy to balance radiative losses (e.g., [49,164]). As such, the onset of wave-driven turbulence is likely to be essential for any significant oscillatory-powered heating in the corona.

The physical processes that produce wave-driven turbulence are robust in a large variety of situations, such as different types of structures, different field line lengths, propagating and standing waves, etc. Despite this, observational evidence for the formation of TWIKH rolls in the corona remains very limited. A probable cause for this is due to the technological constraints of current observational facilities, and, in particular, limitations on the spatial resolution. With state-of-the-art instruments, high-resolution imaging is increasing in availability (e.g., DKIST, Solar Orbiter and Hi-C sounding rocket flights). However, even now, spatial scales approaching the dissipation length scale are well beyond reach. Indirect indicators of turbulence (e.g., non-thermal line broadening) and/or interpretations of decayless oscillations, as evidence of transverse wave-driven turbulence, are providing some insight, but the nature of turbulence (or non-existence) in coronal plasma remains uncertain. Indeed, ref. [165] recently argued that the corona is not in a turbulent state.

A potential inhibitor of wave-driven turbulence in the corona is the tension force associated with the magnetic field. In particular, a component of the field parallel (or anti-parallel) to the velocity shear flow can provide a large stabilising force that significantly reduces the instability growth rate and, thus, greatly reduces plasma mixing. The exact nature of the coronal field remains unclear but a large group of coronal heating models require a proliferation of current sheets which must be associated with a complex and convoluted field. It remains uncertain whether the instabilities discussed above are able to fully develop in a much more inhomogeneous field. Certainly, in this state, wave processes such as phase-mixing can still enhance the rate of wave dissipation. However, for observed wave amplitudes, this enhancement may still be insufficient to generate high heating rates [109]. As the development of wave-driven turbulence is associated with significant consequences for wave energy estimates and seismological inversions, it is imperative to determine whether it is ubiquitous in the corona.

Funding: This research was funded by the European Research Council, grant number 647214.

Institutional Review Board Statement: Not applicable.

Informed Consent Statement: Not applicable.

Data Availability Statement: Not applicable.

Conflicts of Interest: The author declares no conflict of interest.

Abbreviations

The following abbreviations are used in this manuscript:

KHI	Kelvin–Helmholtz instability
DEM	Differential Emission Measure
LoS	Line of Sight

References

1. Alfvén, H. Existence of Electromagnetic-Hydrodynamic Waves. *Nature* **1942**, *150*, 405–406. [CrossRef]
2. Basu, S. Global seismology of the Sun. *Living Rev. Sol. Phys.* **2016**, *13*, 2. [CrossRef]

3. Jess, D.B.; Van Doorsselaere, T.; Verth, G.; Fedun, V.; Krishna Prasad, S.; Erdélyi, R.; Keys, P.H.; Grant, S.D.T.; Uitenbroek, H.; Christian, D.J. An Inside Look at Sunspot Oscillations with Higher Azimuthal Wavenumbers. *Astrophys. J.* **2017**, *842*, 59. [CrossRef]
4. De Pontieu, B.; McIntosh, S.W.; Carlsson, M.; Hansteen, V.H.; Tarbell, T.D.; Schrijver, C.J.; Title, A.M.; Shine, R.A.; Tsuneta, S.; Katsukawa, Y.; et al. Chromospheric Alfvénic Waves Strong Enough to Power the Solar Wind. *Science* **2007**, *318*, 1574–1577. [CrossRef]
5. Zaqarashvili, T.V.; Erdélyi, R. Oscillations and Waves in Solar Spicules. *Space Sci. Rev.* **2009**, *149*, 355–388. [CrossRef]
6. Aschwanden, M.J.; Fletcher, L.; Schrijver, C.J.; Alexander, D. Coronal Loop Oscillations Observed with the Transition Region and Coronal Explorer. *Astrophys. J.* **1999**, *520*, 880–894. [CrossRef]
7. Tomczyk, S.; McIntosh, S.W.; Keil, S.L.; Judge, P.G.; Schad, T.; Seeley, D.H.; Edmondson, J. Alfvén Waves in the Solar Corona. *Science* **2007**, *317*, 1192–1196. [CrossRef]
8. Tu, C.Y.; Marsch, E. Magnetohydrodynamic Structures Waves and Turbulence in the Solar Wind: Observations and Theories. *Space Sci. Rev.* **1995**, *73*, 1–210. [CrossRef]
9. Khotyaintsev, Y.V.; Graham, D.B.; Vaivads, A.; Steinvall, K.; Edberg, N.J.T.; Eriksson, A.I.; Johansson, E.P.G.; Sorriso-Valvo, L.; Maksimovic, M.; Bale, S.D.; et al. Density Fluctuations Associated with Turbulence and Waves: First Observations by Solar Orbiter. *arXiv* **2021**, arXiv:2103.17208.
10. Klimchuk, J.A. On Solving the Coronal Heating Problem. *Sol. Phys.* **2006**, *234*, 41–77. [CrossRef]
11. Erdélyi, R.; Ballai, I. Heating of the solar and stellar coronae: A review. *Astron. Nachrichten* **2007**, *328*, 726–733. [CrossRef]
12. Parnell, C.E.; De Moortel, I. A contemporary view of coronal heating. *Philos. Trans. R. Soc. Lond. Ser. A* **2012**, *370*, 3217–3240. [CrossRef] [PubMed]
13. Reale, F. Coronal Loops: Observations and Modeling of Confined Plasma. *Living Rev. Sol. Phys.* **2014**, *11*, 4. [CrossRef] [PubMed]
14. Arregui, I. Wave heating of the solar atmosphere. *Philos. Trans. R. Soc. Lond. Ser. A* **2015**, *373*, 20140261. [CrossRef]
15. Wilmot-Smith, A.L. An overview of flux braiding experiments. *Philos. Trans. R. Soc. Lond. Ser. A* **2015**, *373*, 20140265. [CrossRef] [PubMed]
16. Van Doorsselaere, T.; Srivastava, A.K.; Antolin, P.; Magyar, N.; Vasheghani Farahani, S.; Tian, H.; Kolotkov, D.; Ofman, L.; Guo, M.; Arregui, I.; et al. Coronal Heating by MHD Waves. *Space Sci. Rev.* **2020**, *216*, 140. [CrossRef]
17. Viall, N.M.; De Moortel, I.; Downs, C.; Klimchuk, J.A.; Parenti, S.; Reale, F. The Heating of the Solar Corona. *Sol. Phys. Sol. Wind.* **2021**, *1*, 35. [CrossRef]
18. Matthaeus, W.H.; Lamkin, S.L. Turbulent magnetic reconnection. *Phys. Fluids* **1986**, *29*, 2513–2534. [CrossRef]
19. Lazarian, A.; Vishniac, E.T. Reconnection in a Weakly Stochastic Field. *Astrophyis. J.* **1999**, *517*, 700–718. [CrossRef]
20. Servidio, S.; Dmitruk, P.; Greco, A.; Wan, M.; Donato, S.; Cassak, P.A.; Shay, M.A.; Carbone, V.; Matthaeus, W.H. Magnetic reconnection as an element of turbulence. *Nonlinear Process. Geophys.* **2011**, *18*, 675–695. [CrossRef]
21. Handy, B.N.; Acton, L.W.; Kankelborg, C.C.; Wolfson, C.J.; Akin, D.J.; Bruner, M.E.; Caravalho, R.; Catura, R.C.; Chevalier, R.; Duncan, D.W.; et al. The transition region and coronal explorer. *Sol. Phys.* **1999**, *187*, 229–260. [CrossRef]
22. Nakariakov, V.M.; Ofman, L.; Deluca, E.E.; Roberts, B.; Davila, J.M. TRACE observation of damped coronal loop oscillations: Implications for coronal heating. *Science* **1999**, *285*, 862–864. [CrossRef] [PubMed]
23. Aschwanden, M.J.; de Pontieu, B.; Schrijver, C.J.; Title, A.M. Transverse Oscillations in Coronal Loops Observed with TRACE II. Measurements of Geometric and Physical Parameters. *Sol. Phys.* **2002**, *206*, 99–132. [CrossRef]
24. Okamoto, T.J.; Tsuneta, S.; Berger, T.E.; Ichimoto, K.; Katsukawa, Y.; Lites, B.W.; Nagata, S.; Shibata, K.; Shimizu, T.; Shine, R.A.; et al. Coronal Transverse Magnetohydrodynamic Waves in a Solar Prominence. *Science* **2007**, *318*, 1577–1580. [CrossRef] [PubMed]
25. Antolin, P.; Verwichte, E. Transverse Oscillations of Loops with Coronal Rain Observed by Hinode/Solar Optical Telescope. *Astrophys. J.* **2011**, *736*, 121. [CrossRef]
26. McIntosh, S.W.; de Pontieu, B.; Carlsson, M.; Hansteen, V.; Boerner, P.; Goossens, M. Alfvénic waves with sufficient energy to power the quiet solar corona and fast solar wind. *Nature* **2011**, *475*, 477–480. [CrossRef]
27. Morton, R.J.; Verth, G.; Hillier, A.; Erdélyi, R. The Generation and Damping of Propagating MHD Kink Waves in the Solar Atmosphere. *Astrophys. J.* **2014**, *784*, 29. [CrossRef]
28. Morton, R.J.; Tomczyk, S.; Pinto, R. Investigating Alfvénic wave propagation in coronal open-field regions. *Nat. Commun.* **2015**, *6*, 7813. [CrossRef]
29. Schrijver, C.J.; Aschwanden, M.J.; Title, A.M. Transverse oscillations in coronal loops observed with TRACE I. An Overview of Events, Movies, and a Discussion of Common Properties and Required Conditions. *Sol. Phys.* **2002**, *206*, 69–98.:1014957715396. [CrossRef]
30. Nakariakov, V.M.; Verwichte, E. Coronal Waves and Oscillations. *Living Rev. Sol. Phys.* **2005**, *2*, 3. [CrossRef]
31. Ruderman, M.S.; Erdélyi, R. Transverse Oscillations of Coronal Loops. *Space Sci. Rev.* **2009**, *149*, 199–228. [CrossRef]
32. Nakariakov, V.M.; Anfinogentov, S.A.; Antolin, P.; Jain, R.; Kolotkov, D.Y.; Kupriyanova, E.G.; Li, D.; Magyar, N.; Nisticò, G.; Pascoe, D.J.; et al. Kink Oscillations of Coronal Loops. *Space Sci. Rev.* **2021**, *217*, 73. [CrossRef]
33. Ionson, J.A. Resonant absorption of Alfvenic surface waves and the heating of solar coronal loops. *Astrophys. J.* **1978**, *226*, 650–673. [CrossRef]
34. Ruderman, M.S.; Roberts, B. The Damping of Coronal Loop Oscillations. *Astrophys. J.* **2002**, *577*, 475–486. [CrossRef]

35. Arregui, I.; Andries, J.; Van Doorsselaere, T.; Goossens, M.; Poedts, S. MHD seismology of coronal loops using the period and damping of quasi-mode kink oscillations. *Astron. Astrophys.* **2007**, *463*, 333–338. [CrossRef]
36. De Moortel, I.; Nakariakov, V.M. Magnetohydrodynamic waves and coronal seismology: An overview of recent results. *Philos. Trans. R. Soc. Lond. Ser. A* **2012**, *370*, 3193–3216. [CrossRef]
37. Pascoe, D.J.; Goddard, C.R.; Nisticò, G.; Anfinogentov, S.; Nakariakov, V.M. Coronal loop seismology using damping of standing kink oscillations by mode coupling. *Astron. Astrophys.* **2016**, *589*, A136. [CrossRef]
38. Duckenfield, T.; Kolotkov, D. Coronal seismology at 20. *Astron. Geophys.* **2021**, *62*, 3–28. [CrossRef]
39. Terradas, J.; Oliver, R.; Ballester, J.L. Damped Coronal Loop Oscillations: Time-dependent Results. *Astrophys. J.* **2006**, *642*, 533–540. [CrossRef]
40. Pascoe, D.J.; Wright, A.N.; De Moortel, I. Coupled Alfvén and Kink Oscillations in Coronal Loops. *Astrophys. J.* **2010**, *711*, 990–996. [CrossRef]
41. Davila, J.M. Heating of the Solar Corona by the Resonant Absorption of Alfven Waves. *Astrophys. J.* **1987**, *317*, 514. [CrossRef]
42. Poedts, S.; Goossens, M.; Kerner, W. On the Efficiency of Coronal Loop Heating by Resonant Absorption. *Astrophys. J.* **1990**, *360*, 279. [CrossRef]
43. Beliën, A.J.C.; Martens, P.C.H.; Keppens, R. Coronal Heating by Resonant Absorption: The Effects of Chromospheric Coupling. *Astrophys. J.* **1999**, *526*, 478–493. [CrossRef]
44. Pagano, P.; De Moortel, I. Contribution of mode-coupling and phase-mixing of Alfvén waves to coronal heating. *Astron. Astrophys.* **2017**, *601*, A107. [CrossRef]
45. Heyvaerts, J.; Priest, E.R. Coronal heating by phase-mixed shear Alfven waves. *Astron. Astrophys.* **1983**, *117*, 220–234.
46. Ofman, L.; Davila, J.M. Alfvén wave heating of coronal holes and the relation to the high-speed solar wind. *J. Geophys. Res.* **1995**, *100*, 23413–23426. [CrossRef]
47. Hood, A.W.; Ireland, J.; Priest, E.R. Heating of coronal holes by phase mixing. *Astron. Astrophys.* **1997**, *318*, 957–962.
48. De Moortel, I.; Hood, A.W.; Ireland, J.; Arber, T.D. Phase mixing of Alfvén waves in a stratified and open atmosphere. *Astron. Astrophys.* **1999**, *346*, 641–651.
49. Pagano, P.; Pascoe, D.J.; De Moortel, I. Contribution of phase-mixing of Alfvén waves to coronal heating in multi-harmonic loop oscillations. *Astron. Astrophys.* **2018**, *616*, A125. [CrossRef]
50. Pagano, P.; De Moortel, I. Contribution of observed multi frequency spectrum of Alfvén waves to coronal heating. *Astron. Astrophys.* **2019**, *623*, A37. [CrossRef]
51. Chandrasekhar, S. *Hydrodynamic and Hydromagnetic Stability*; International Series of Monographs on Physics; Clarendon: Oxford, UK, 1961.
52. Roberts, B. On the hydromagnetic stability of an unsteady Kelvin-Helmholtz flow. *J. Fluid Mech.* **1973**, *59*, 65–76. [CrossRef]
53. Browning, P.K.; Priest, E.R. Kelvin-Helmholtz instability of a phased-mixed Alfven wave. *Astron. Astrophys.* **1984**, *131*, 283–290.
54. Terradas, J.; Andries, J.; Goossens, M.; Arregui, I.; Oliver, R.; Ballester, J.L. Nonlinear Instability of Kink Oscillations due to Shear Motions. *Astrophys. J.* **2008**, *687*, L115. [CrossRef]
55. Zaqarashvili, T.V.; Zhelyazkov, I.; Ofman, L. Stability of Rotating Magnetized Jets in the Solar Atmosphere. I. Kelvin-Helmholtz Instability. *Astrophys. J.* **2015**, *813*, 123. [CrossRef]
56. Hillier, A.; Barker, A.; Arregui, I.; Latter, H. On Kelvin-Helmholtz and parametric instabilities driven by coronal waves. *Mon. Not. R. Astron. Soc.* **2019**, *482*, 1143–1153. [CrossRef]
57. Wang, T.; Ofman, L.; Davila, J.M.; Su, Y. Growing Transverse Oscillations of a Multistranded Loop Observed by SDO/AIA. *Astrophys. J.* **2012**, *751*, L27. [CrossRef]
58. Tian, H.; McIntosh, S.W.; Wang, T.; Ofman, L.; De Pontieu, B.; Innes, D.E.; Peter, H. Persistent Doppler Shift Oscillations Observed with Hinode/EIS in the Solar Corona: Spectroscopic Signatures of Alfvénic Waves and Recurring Upflows. *Astrophys. J.* **2012**, *759*, 144. [CrossRef]
59. Nisticò, G.; Nakariakov, V.M.; Verwichte, E. Decaying and decayless transverse oscillations of a coronal loop. *Astron. Astrophys.* **2013**, *552*, A57. [CrossRef]
60. Anfinogentov, S.A.; Nakariakov, V.M.; Nisticò, G. Decayless low-amplitude kink oscillations: A common phenomenon in the solar corona? *Astron. Astrophys.* **2015**, *583*, A136. [CrossRef]
61. Duckenfield, T.; Anfinogentov, S.A.; Pascoe, D.J.; Nakariakov, V.M. Detection of the Second Harmonic of Decay-less Kink Oscillations in the Solar Corona. *Astrophys. J. Lett.* **2018**, *854*, L5. [CrossRef]
62. Mandal, S.; Tian, H.; Peter, H. Flare-induced decay-less transverse oscillations in solar coronal loops. *Astron. Astrophys.* **2021**, *652*, L3. [CrossRef]
63. Antolin, P.; De Moortel, I.; Van Doorsselaere, T.; Yokoyama, T. Modeling Observed Decay-less Oscillations as Resonantly Enhanced Kelvin-Helmholtz Vortices from Transverse MHD Waves and Their Seismological Application. *Astrophys. J.* **2016**, *830*, L22. [CrossRef]
64. Thurgood, J.O.; Morton, R.J.; McLaughlin, J.A. First Direct Measurements of Transverse Waves in Solar Polar Plumes Using SDO/AIA. *Astrophys. J.* **2014**, *790*, L2. [CrossRef]
65. Pant, V.; Van Doorsselaere, T. Revisiting the Relation between Nonthermal Line Widths and Transverse MHD Wave Amplitudes. *Astrophys. J.* **2020**, *899*, 1. [CrossRef]

66. Fyfe, L.; Howson, T.; De Moortel, I.; Pant, V.; Van Doorsselaere, T. Investigating coronal wave energy estimates using synthetic non-thermal line widths. *arXiv* **2021**, arXiv:2110.00257.
67. Withbroe, G.L.; Noyes, R.W. Mass and energy flow in the solar chromosphere and corona. *Annu. Rev. Astron. Astrophys.* **1977**, *15*, 363–387. [CrossRef]
68. McLaughlin, J.A.; Hood, A.W.; de Moortel, I. Review Article: MHD Wave Propagation Near Coronal Null Points of Magnetic Fields. *Space Sci. Rev.* **2011**, *158*, 205–236. [CrossRef]
69. McLaughlin, J.A. Phase Mixing of Alfvén Waves Near a 2D Magnetic Null Point. *J. Astrophys. Astron.* **2013**, *34*, 223–246. [CrossRef]
70. Prokopyszyn, A.P.K.; Hood, A.W.; De Moortel, I. Phase mixing of nonlinear Alfvén waves. *Astron. Astrophys.* **2019**, *624*, A90. [CrossRef]
71. Prokopyszyn, A.P.K.; Hood, A.W. Investigating the damping rate of phase-mixed Alfvén waves. *Astron. Astrophys.* **2019**, *632*, A93. [CrossRef]
72. Prokopyszyn, A.P.K. Magnetohydrodynamic Waves in the Solar Corona. Ph.D. Thesis, University of St Andrews, St Andrews, UK, 2021.
73. Howson, T.; De Moortel, I. The effects of driving time scales on coronal heating in a stratified atmosphere. **2022**, in preparation.
74. Howson, T.A.; De Moortel, I.; Fyfe, L.E. The effects of driving time scales on heating in a coronal arcade. *Astron. Astrophys.* **2020**, *643*, A85. [CrossRef]
75. Ryutov, D.A.; Ryutova, M.P. Sound oscillations in a plasma with "magnetic filaments". *Sov. J. Exp. Theor. Phys.* **1976**, *43*, 491–497.
76. Ofman, L.; Davila, J.M.; Steinolfson, R.S. Coronal Heating by the Resonant Absorption of Alfven Waves: The Effect of Viscous Stress Tensor. *Astrophys. J.* **1994**, *421*, 360. [CrossRef]
77. Goossens, M.; Andries, J.; Aschwanden, M.J. Coronal loop oscillations. An interpretation in terms of resonant absorption of quasi-mode kink oscillations. *Astron. Astrophys.* **2002**, *394*, L39–L42. [CrossRef]
78. Pascoe, D.J.; Hood, A.W.; De Moortel, I.; Wright, A.N. Damping of kink waves by mode coupling. II. Parametric study and seismology. *Astron. Astrophys.* **2013**, *551*, A40. [CrossRef]
79. Ruderman, M.S. The resonant damping of oscillations of coronal loops with elliptic cross-sections. *Astron. Astrophys.* **2003**, *409*, 287–297. [CrossRef]
80. Andries, J.; Goossens, M.; Hollweg, J.V.; Arregui, I.; Van Doorsselaere, T. Coronal loop oscillations. Calculation of resonantly damped MHD quasi-mode kink oscillations of longitudinally stratified loops. *Astron. Astrophys.* **2005**, *430*, 1109–1118. [CrossRef]
81. Terradas, J.; Oliver, R.; Ballester, J.L. Damping of Kink Oscillations in Curved Coronal Loops. *Astrophys. J. Letts.* **2006**, *650*, L91–L94. [CrossRef]
82. Giagkiozis, I.; Goossens, M.; Verth, G.; Fedun, V.; Van Doorsselaere, T. Resonant Absorption of Axisymmetric Modes in Twisted Magnetic Flux Tubes. *Astrophys. J.* **2016**, *823*, 71. [CrossRef]
83. Howson, T.A.; De Moortel, I.; Antolin, P.; Van Doorsselaere, T.; Wright, A.N. Resonant absorption in expanding coronal magnetic flux tubes with uniform density. *Astron. Astrophys.* **2019**, *631*, A105. [CrossRef]
84. Guo, M.; Li, B.; Van Doorsselaere, T. Kink Oscillations in Solar Coronal Loops with Elliptical Cross Sections. I. The Linear Regime. *Astrophys. J.* **2020**, *904*, 116. [CrossRef]
85. Howson, T.; De Moortel, I.; Pontin, D. Magnetic reconnection and the Kelvin-Helmholtz instability in the solar corona. *arXiv* **2021**, arXiv:2109.15019.
86. Antolin, P.; Yokoyama, T.; Van Doorsselaere, T. Fine Strand-like Structure in the Solar Corona from Magnetohydrodynamic Transverse Oscillations. *Astrophys. J. Letts.* **2014**, *787*, L22. [CrossRef]
87. Antolin, P.; Okamoto, T.J.; De Pontieu, B.; Uitenbroek, H.; Van Doorsselaere, T.; Yokoyama, T. Resonant Absorption of Transverse Oscillations and Associated Heating in a Solar Prominence. II. Numerical Aspects. *Astrophys. J.* **2015**, *809*, 72. [CrossRef]
88. Antolin, P.; Schmit, D.; Pereira, T.M.D.; De Pontieu, B.; De Moortel, I. Transverse Wave Induced Kelvin-Helmholtz Rolls in Spicules. *Astrophys. J.* **2018**, *856*, 44. [CrossRef]
89. Guo, M.; Van Doorsselaere, T.; Karampelas, K.; Li, B. Wave Heating in Simulated Multistranded Coronal Loops. *Astrophys. J.* **2019**, *883*, 20. [CrossRef]
90. Magyar, N.; Van Doorsselaere, T.; Marcu, A. Numerical simulations of transverse oscillations in radiatively cooling coronal loops. *Astron. Astrophys.* **2015**, *582*, A117. [CrossRef]
91. Karampelas, K.; Van Doorsselaere, T.; Guo, M. Wave heating in gravitationally stratified coronal loops in the presence of resistivity and viscosity. *Astron. Astrophys.* **2019**, *623*, A53. [CrossRef]
92. Van Doorsselaere, T.; Andries, J.; Poedts, S. Observational evidence favors a resistive wave heating mechanism for coronal loops over a viscous phenomenon. *Astron. Astrophys.* **2007**, *471*, 311–314.:20066658. [CrossRef]
93. Karampelas, K.; Van Doorsselaere, T. Simulations of fully deformed oscillating flux tubes. *Astron. Astrophys.* **2018**, *610*, L9. [CrossRef]
94. Karampelas, K.; Van Doorsselaere, T.; Antolin, P. Heating by transverse waves in simulated coronal loops. *Astron. Astrophys.* **2017**, *604*, A130. [CrossRef]
95. Hillier, A.; Arregui, I. Coronal Cooling as a Result of Mixing by the Nonlinear Kelvin-Helmholtz Instability. *Astrophys. J.* **2019**, *885*, 101. [CrossRef]
96. Edwin, P.M.; Roberts, B. Wave Propagation in a Magnetic Cylinder. *Sol. Phys.* **1983**, *88*, 179–191. [CrossRef]

97. Shi, M.; Van Doorsselaere, T.; Guo, M.; Karampelas, K.; Li, B.; Antolin, P. The First 3D Coronal Loop Model Heated by MHD Waves against Radiative Losses. *Astrophys. J.* **2021**, *908*, 233. [CrossRef]
98. Hillier, A.; Van Doorsselaere, T.; Karampelas, K. Estimating the Energy Dissipation from Kelvin-Helmholtz Instability Induced Turbulence in Oscillating Coronal Loops. *Astrophys. J.* **2020**, *897*, L13. [CrossRef]
99. Afanasyev, A.; Karampelas, K.; Van Doorsselaere, T. Coronal Loop Transverse Oscillations Excited by Different Driver Frequencies. *Astrophys. J.* **2019**, *876*, 100. [CrossRef]
100. Karampelas, K.; Van Doorsselaere, T. Generating Transverse Loop Oscillations through a Steady-flow Driver. *Astrophys. J.* **2020**, *897*, L35. [CrossRef]
101. Karampelas, K.; Van Doorsselaere, T. Transverse Loop Oscillations via Vortex Shedding: A Self-oscillating Process. *Astrophys. J.* **2021**, *908*, L7. [CrossRef]
102. Magyar, N.; Van Doorsselaere, T. Damping of nonlinear standing kink oscillations: A numerical study. *Astron. Astrophys.* **2016**, *595*, A81. [CrossRef]
103. Antolin, P.; Van Doorsselaere, T. Influence of resonant absorption on the generation of the Kelvin-Helmholtz Instability. *Front. Phys.* **2019**, *7*, 85. [CrossRef]
104. Howson, T.A.; De Moortel, I.; Antolin, P. The effects of resistivity and viscosity on the Kelvin- Helmholtz instability in oscillating coronal loops. *Astron. Astrophys.* **2017**, *602*, A74. [CrossRef]
105. Howson, T.A.; De Moortel, I.; Antolin, P. Energetics of the Kelvin-Helmholtz instability induced by transverse waves in twisted coronal loops. *Astron. Astrophys.* **2017**, *607*, A77. [CrossRef]
106. Terradas, J.; Magyar, N.; Van Doorsselaere, T. Effect of Magnetic Twist on Nonlinear Transverse Kink Oscillations of Line-tied Magnetic Flux Tubes. *Astrophys. J.* **2018**, *853*, 35. [CrossRef]
107. Barbulescu, M.; Ruderman, M.S.; Van Doorsselaere, T.; Erdélyi, R. An Analytical Model of the Kelvin-Helmholtz Instability of Transverse Coronal Loop Oscillations. *Astrophys. J.* **2019**, *870*, 108. [CrossRef]
108. Parker, E.N. Topological Dissipation and the Small-Scale Fields in Turbulent Gases. *Astrophys. J.* **1972**, *174*, 499. [CrossRef]
109. Howson, T.A.; De Moortel, I.; Reid, J. Phase mixing and wave heating in a complex coronal plasma. *Astron. Astrophys.* **2020**, *636*, A40. [CrossRef]
110. Goddard, C.R.; Nisticò, G. Temporal evolution of oscillating coronal loops. *Astron. Astrophys.* **2020**, *638*, A89. [CrossRef]
111. Antolin, P.; De Moortel, I.; Van Doorsselaere, T.; Yokoyama, T. Observational Signatures of Transverse Magnetohydrodynamic Waves and Associated Dynamic Instabilities in Coronal Flux Tubes. *Astrophys. J.* **2017**, *836*, 219. [CrossRef]
112. Karampelas, K.; Van Doorsselaere, T.; Pascoe, D.J.; Guo, M.; Antolin, P. Amplitudes and energy fluxes of simulated decayless kink oscillations. *Front. Astron. Space Sci.* **2019**, *6*, 38. [CrossRef]
113. Shi, M.; Van Doorsselaere, T.; Antolin, P.; Li, B. Forward Modeling of Simulated Transverse Oscillations in Coronal Loops and the Influence of Background Emission. *arXiv* **2021**, arXiv:2109.02338.
114. Van Doorsselaere, T.; Antolin, P.; Karampelas, K. Broadening of the differential emission measure by multi-shelled and turbulent loops. *Astron. Astrophys.* **2018**, *620*, A65. [CrossRef]
115. Brooks, D.H.; Warren, H.P.; Ugarte-Urra, I. Solar Coronal Loops Resolved by Hinode and the Solar Dynamics Observatory. *Astrophys. J.* **2012**, *755*, L33. [CrossRef]
116. Viall, N.M.; Klimchuk, J.A. Modeling the Line-of-sight Integrated Emission in the Corona: Implications for Coronal Heating. *Astrophys. J.* **2013**, *771*, 115. [CrossRef]
117. Magyar, N.; Van Doorsselaere, T. The Instability and Non-existence of Multi-stranded Loops When Driven by Transverse Waves. *Astrophys. J.* **2016**, *823*, 82. [CrossRef]
118. Okamoto, T.J.; Antolin, P.; De Pontieu, B.; Uitenbroek, H.; Van Doorsselaere, T.; Yokoyama, T. Resonant Absorption of Transverse Oscillations and Associated Heating in a Solar Prominence. I. Observational Aspects. *Astrophys. J.* **2015**, *809*, 71. [CrossRef]
119. He, J.S.; Tu, C.Y.; Marsch, E.; Guo, L.J.; Yao, S.; Tian, H. Upward propagating high-frequency Alfvén waves as identified from dynamic wave-like spicules observed by SOT on Hinode. *Astron. Astrophys.* **2009**, *497*, 525–535. [CrossRef]
120. Okamoto, T.J.; De Pontieu, B. Propagating Waves Along Spicules. *Astrophys. J. Letts.* **2011**, *736*, L24. [CrossRef]
121. Verth, G.; Terradas, J.; Goossens, M. Observational Evidence of Resonantly Damped Propagating Kink Waves in the Solar Corona. *Astrophys. J. Letts.* **2010**, *718*, L102–L105. [CrossRef]
122. Tiwari, A.K.; Morton, R.J.; Régnier, S.; McLaughlin, J.A. Damping of Propagating Kink Waves in the Solar Corona. *Astrophys. J.* **2019**, *876*, 106. [CrossRef]
123. Iroshnikov, P.S. Turbulence of a Conducting Fluid in a Strong Magnetic Field. *Sov. Astron.* **1964**, *7*, 566.
124. Kraichnan, R.H. Inertial-Range Spectrum of Hydromagnetic Turbulence. *Phys. Fluids* **1965**, *8*, 1385–1387. [CrossRef]
125. Goldreich, P.; Sridhar, S. Toward a Theory of Interstellar Turbulence. II. Strong Alfvenic Turbulence. *Astrophys. J.* **1995**, *438*, 763. [CrossRef]
126. Goldreich, P.; Sridhar, S. Magnetohydrodynamic Turbulence Revisited. *Astrophys. J.* **1997**, *485*, 680–688. [CrossRef]
127. Chandran, B.D.G. Weak Compressible Magnetohydrodynamic Turbulence in the Solar Corona. *Phys. Rev. Lett.* **2005**, *95*, 265004. [CrossRef]
128. van Ballegooijen, A.A.; Asgari-Targhi, M.; Cranmer, S.R.; DeLuca, E.E. Heating of the Solar Chromosphere and Corona by Alfvén Wave Turbulence. *Astrophys. J.* **2011**, *736*, 3. [CrossRef]

129. Howes, G.G.; Nielson, K.D. Alfvén wave collisions, the fundamental building block of plasma turbulence. I. Asymptotic solution. *Phys. Plasmas* **2013**, *20*, 072302. [CrossRef]
130. Matthaeus, W.H.; Zank, G.P.; Oughton, S.; Mullan, D.J.; Dmitruk, P. Coronal Heating by Magnetohydrodynamic Turbulence Driven by Reflected Low-Frequency Waves. *Astrophys. J. Letts.* **1999**, *523*, L93–L96. [CrossRef]
131. Dmitruk, P.; Matthaeus, W.H.; Milano, L.J.; Oughton, S. Conditions for sustainment of magnetohydrodynamic turbulence driven by Alfvén waves. *Phys. Plasmas* **2001**, *8*, 2377–2384. [CrossRef]
132. Verdini, A.; Velli, M. Alfvén Waves and Turbulence in the Solar Atmosphere and Solar Wind. *Astrophys. J.* **2007**, *662*, 669–676. [CrossRef]
133. Cranmer, S.R.; van Ballegooijen, A.A.; Edgar, R.J. Self-consistent Coronal Heating and Solar Wind Acceleration from Anisotropic Magnetohydrodynamic Turbulence. *Astrophys. J.* **2007**, *171*, 520–551. [CrossRef]
134. Chandran, B.D.G.; Hollweg, J.V. Alfvén Wave Reflection and Turbulent Heating in the Solar Wind from 1 Solar Radius to 1 AU: An Analytical Treatment. *Astrophys. J.* **2009**, *707*, 1659–1667. [CrossRef]
135. Matsumoto, T.; Suzuki, T.K. Connecting the Sun and the Solar Wind: The First 2.5-dimensional Self-consistent MHD Simulation under the Alfvén Wave Scenario. *Astrophys. J.* **2012**, *749*, 8. [CrossRef]
136. Matsumoto, T.; Suzuki, T.K. Connecting the Sun and the solar wind: The self-consistent transition of heating mechanisms. *Mon. Not. R. Astron. Soc.* **2014**, *440*, 971–986. [CrossRef]
137. Lionello, R.; Velli, M.; Downs, C.; Linker, J.A.; Mikić, Z.; Verdini, A. Validating a Time-dependent Turbulence-driven Model of the Solar Wind. *Astrophys. J.* **2014**, *784*, 120. [CrossRef]
138. van der Holst, B.; Sokolov, I.V.; Meng, X.; Jin, M.; Manchester, W.B., IV; Tóth, G.; Gombosi, T.I. Alfvén Wave Solar Model (AWSoM): Coronal Heating. *Astrophys. J.* **2014**, *782*, 81. [CrossRef]
139. van Ballegooijen, A.A.; Asgari-Targhi, M. Heating and Acceleration of the Fast Solar Wind by Alfvén Wave Turbulence. *Astrophys. J.* **2016**, *821*, 106. [CrossRef]
140. Asgari-Targhi, M.; Asgari-Targhi, A.; Hahn, M.; Savin, D.W. Effects of Density Fluctuations on Alfvén Wave Turbulence in a Coronal Hole. *Astrophys. J.* **2021**, *911*, 63. [CrossRef]
141. Ofman, L. Wave Modeling of the Solar Wind. *Living Rev. Sol. Phys.* **2010**, *7*, 4. [CrossRef]
142. Cranmer, S.R.; Asgari-Targhi, M.; Miralles, M.P.; Raymond, J.C.; Strachan, L.; Tian, H.; Woolsey, L.N. The role of turbulence in coronal heating and solar wind expansion. *Philos. Trans. R. Soc. Lond. Ser. A* **2015**, *373*, 20140148. [CrossRef]
143. Banerjee, D.; Krishna Prasad, S.; Pant, V.; McLaughlin, J.A.; Antolin, P.; Magyar, N.; Ofman, L.; Tian, H.; Van Doorsselaere, T.; De Moortel, I.; Wang, T.J. Magnetohydrodynamic Waves in Open Coronal Structures. *Space Sci. Rev.* **2021**, *217*, 76. [CrossRef]
144. Bruno, R.; Carbone, V. The Solar Wind as a Turbulence Laboratory. *Living Rev. Sol. Phys.* **2013**, *10*, 2. [CrossRef]
145. Matthaeus, W.H.; Goldstein, M.L. Measurement of the rugged invariants of magnetohydrodynamic turbulence in the solar wind. *J. Geophys. Res.* **1982**, *87*, 6011–6028. [CrossRef]
146. Zank, G.P.; Matthaeus, W.H.; Smith, C.W. Evolution of turbulent magnetic fluctuation power with heliospheric distance. *J. Geophys. Res.* **1996**, *101*, 17093–17108. [CrossRef]
147. Bavassano, B.; Pietropaolo, E.; Bruno, R. Alfvénic turbulence in the polar wind: A statistical study on cross helicity and residual energy variations. *J. Geophys. Res.* **2000**, *105*, 12697–12704. [CrossRef]
148. Boldyrev, S.; Perez, J.C.; Borovsky, J.E.; Podesta, J.J. Spectral Scaling Laws in Magnetohydrodynamic Turbulence Simulations and in the Solar Wind. *Astrophys. J. Letts.* **2011**, *741*, L19. [CrossRef]
149. Borovsky, J.E. The velocity and magnetic field fluctuations of the solar wind at 1 AU: Statistical analysis of Fourier spectra and correlations with plasma properties. *J. Geophys. Res. (Space Phys.)* **2012**, *117*, A05104. [CrossRef]
150. Andrés, N.; Sahraoui, F.; Hadid, L.Z.; Huang, S.Y.; Romanelli, N.; Galtier, S.; DiBraccio, G.; Halekas, J. The Evolution of Compressible Solar Wind Turbulence in the Inner Heliosphere: PSP, THEMIS, and MAVEN Observations. *Astrophys. J.* **2021**, *919*, 19. [CrossRef]
151. Kieokaew, R.; Lavraud, B.; Yang, Y.; Matthaeus, W.H.; Ruffolo, D.; Stawarz, J.E.; Aizawa, S.; Foullon, C.; Génot, V.; Pinto, R.F.; et al. Solar Orbiter Observations of the Kelvin-Helmholtz Instability in the Solar Wind. *arXiv* **2021**, arXiv:2103.15489.
152. Telloni, D.; Sorriso-Valvo, L.; Woodham, L.D.; Panasenco, O.; Velli, M.; Carbone, F.; Zank, G.P.; Bruno, R.; Perrone, D.; Nakanotani, M.; et al. Evolution of Solar Wind Turbulence from 0.1 to 1 au during the First Parker Solar Probe-Solar Orbiter Radial Alignment. *Astrophys. J.* **2021**, *912*, L21. [CrossRef]
153. Goossens, M.; Terradas, J.; Andries, J.; Arregui, I.; Ballester, J.L. On the nature of kink MHD waves in magnetic flux tubes. *Astron. Astrophys.* **2009**, *503*, 213–223. [CrossRef]
154. Magyar, N.; Van Doorsselaere, T.; Goossens, M. Generalized phase mixing: Turbulence-like behaviour from unidirectionally propagating MHD waves. *Sci. Rep.* **2017**, *7*, 14820. [CrossRef] [PubMed]
155. Magyar, N.; Van Doorsselaere, T.; Goossens, M. Understanding Uniturbulence: Self-cascade of MHD Waves in the Presence of Inhomogeneities. *Astrophys. J.* **2019**, *882*, 50. [CrossRef]
156. Van Doorsselaere, T.; Li, B.; Goossens, M.; Hnat, B.; Magyar, N. Wave Pressure and Energy Cascade Rate of Kink Waves Computed with Elsässer Variables. *Astrophys. J.* **2020**, *899*, 100. [CrossRef]
157. Elsasser, W.M. The Hydromagnetic Equations. *Phys. Rev.* **1950**, *79*, 183. [CrossRef]
158. Van Doorsselaere, T.; Goossens, M.; Magyar, N.; Ruderman, M.S.; Ismayilli, R. Nonlinear Damping of Standing Kink Waves Computed With Elsässer Variables. *Astrophys. J.* **2021**, *910*, 58. [CrossRef]

159. Verwichte, E.; Van Doorsselaere, T.; White, R.S.; Antolin, P. Statistical seismology of transverse waves in the solar corona. *Astron. Astrophys.* **2013**, *552*, A138. [CrossRef]
160. Goddard, C.R.; Nisticò, G.; Nakariakov, V.M.; Zimovets, I.V. A statistical study of decaying kink oscillations detected using SDO/AIA. *Astron. Astrophys.* **2016**, *585*, A137. [CrossRef]
161. Nechaeva, A.; Zimovets, I.V.; Nakariakov, V.M.; Goddard, C.R. Catalog of Decaying Kink Oscillations of Coronal Loops in the 24th Solar Cycle. *Astrophys. J. Suppl.* **2019**, *241*, 31. [CrossRef]
162. Pagano, P.; De Moortel, I.; Morton, R.J. Effect of coronal loop structure on wave heating through phase mixing. *Astron. Astrophys.* **2020**, *643*, A73. [CrossRef]
163. Cargill, P.J.; De Moortel, I.; Kiddie, G. Coronal Density Structure and its Role in Wave Damping in Loops. *Astrophys. J.* **2016**, *823*, 31. [CrossRef]
164. Van Damme, H.J.; De Moortel, I.; Pagano, P.; Johnston, C.D. Chromospheric evaporation and phase mixing of Alfvén waves in coronal loops. *Astron. Astrophys.* **2020**, *635*, A174. [CrossRef]
165. Klimchuk, J.A.; Antiochos, S.K. How Turbulent is the Magnetically Closed Corona? *Front. Astron. Space Sci.* **2021**, *8*, 83. [CrossRef]